A Low-Profile Pattern Reconfigurable Antenna System
for Automotive MIMO Applications

Jerzy Kowalewski*, Jude Atuegwu, Jonathan Mayer, Tobias Mahler, and Thomas Zwick

Abstract—This paper presents the design and evaluation of a compact antenna system with pattern reconfigurability at 2.6 GHz. The antenna is based on the concept of an electronically steerable parasitic array radiator (ESPAR), and its height is reduced by top loading. The antenna can generate 10 reconfigurable patterns with a maximal gain of 7.4 dBi. Furthermore, a multiple antenna system consisting of these antennas is proposed. The radiation patterns realized by this multiple-input-multiple-output (MIMO) system are optimized for automotive urban scenarios based on the results of previous research. The S-parameter measurement results of a fabricated prototype correlate with the simulation. Furthermore, 3D measurements of radiation patterns correspond very well with simulation and gain up to 8 dBi is obtained.

1. INTRODUCTION

In previous decade the automobile industry developed towards ubiquitous use of diverse wireless services. Modern cars are equipped with antennas for the global system for mobile communications (GSM), long term evolution (LTE), car-to-car communication (C2C), Wi-Fi, satellite navigation systems, satellite radio and remote keyless entry. Most of these antennas are mounted on car-roof inside a shark-fin module. However, as the number of wireless services for cars and the demand on their performance is growing, the volume available for antennas inside these modules gets scarce. Furthermore, not only the number of mobile services is growing but also the number of antennas per service. Automotive MIMO systems [1–4] are proposed to increase the data throughput and to assure continuous reception even if the system is affected by fading. This issue is especially important since mobile communication standards are now being adapted for intelligent transportation systems (ITS) [5, 6] in order to increase road safety and enable autonomous driving in the future. Thus antennas enabling reliable connection with enough data throughput are needed.

A very important issue for an automotive antenna is its radiation characteristic. Currently antennas with omnidirectional radiation are used [2]. At first thought it seems to be the right choice, since signals can impinge the car from all angular directions as the car is moving and changing its driving direction. However, as presented by Reichardt et al. better results can be obtained if antennas have directive patterns [7]. It is shown that due to existence of dominant angles of arrival (AOA) different radiation patterns are advantageous for urban and rural scenarios. In [8] a procedure of antenna synthesis using ray-tracing simulations for multiple antenna systems is presented. Based on this procedure near-optimum vehicular MIMO radiation patterns can be developed. The resulting patterns show increased directivity in the $\pm$ driving direction and the other orthogonal to it (left/right) for the best sub-channels.

A solution offering more flexibility, better performance and coverage of the preferred directions is the use of pattern reconfigurable antennas. There are some major techniques to realize them.

One possibility is switching between radiating elements [10]. Another possibility is switching between different antenna modes [4, 11, 12]. Yet another technique is activation of parasitic elements [13]. The ESPAR (electronically steerable parasitic array radiator) [13] offers very good flexibility in terms of pattern switching. Yet with the diameter of more than $\lambda_0/2$ and height of $\lambda_0/4$ at resonance frequency such an antenna system is bulky. Therefore, it is not applicable for automotive antenna system without further modification.

There are some strict requirements on car-to-infrastructure (C2I) antennas. The design should be compact and possibly low profile in order to fit under the antenna housing. Furthermore, enough bandwidth, moderate gain and 360° view range in azimuth are important for the performance of the system. Some interesting works on MIMO reconfigurable antennas based on parasitic arrays [14, 15] as well as some novel low profile MIMO solutions [16, 17] have been previously proposed in literature. However, the size of [14, 15] hinders their application in automotive systems. Furthermore, the azimuth view range of [15] is not sufficient enough for the application. The gain and bandwidth of antennas [16, 17] are unfortunately not sufficient enough to consider their application in C2I. The focus of this paper is a design of a compact, high-gain automotive antenna based on ESPAR concept. Special attention was given to design of top-hat loading and antenna decoupling structure, thus a broad impedance bandwidth and high antenna efficiency are obtained. To the authors' best knowledge this is the first work presenting detailed design of a MIMO pattern reconfigurable antenna optimized for automotive application.

This paper explains the design procedure of a single reconfigurable antenna in Section 2. This section explains the antenna's switching mechanism as well. In Section 3 the design of a MIMO antenna is discussed. Next, the measurement results are presented and discussed in Section 4. Finally, conclusions are drawn in Section 5.

2. SINGLE RECONFIGURABLE ANTENNA

As discussed in the introduction using antennas with directive radiation patterns can improve the performance of the communication system. This was observed and documented as well in [14]. However even more improvement in the performance can be obtained by switching between these patterns [14]. In [8] an antenna synthesis method is proposed to calculate the optimal radiation characteristics for urban scenarios. The improved synthesis procedure is presented in [9]. Furthermore, the real world dynamic channel measurements are used for the synthesis in this case. In both cases the synthesis results show that optimal patterns cover one the $\pm$ driving direction and the other the left/right direction. These results correspond very well with results from [7]. Therefore, it is anticipated that antennas significantly increases the system performance over an antenna having an omnidirectional pattern and can reduce the number of required antennas. The design frequency is 2.6 GHz which is the center frequency of LTE bands 7 and 38. The last requirement is a compact construction of the MIMO system, thus it can either be installed in a standard automotive antenna housing or in a chassis antenna cavity [18].

2.1. Primary Radiator

In order to reduce antenna height from $\lambda_0/4$ and thus obtain a low-profile antenna, a top-hat monopole is chosen as the primary radiator. It consist of a driven post of height h which is in this case $\lambda_0/10$ and a rectangular metallic hat (see Fig. 1) with diameter p equal to 7.2 mm as capacitive top loading. The driven post is fed directly by inner conductor of a coaxial feed line. Due to the top loading the current has a nearly uniform distribution on the vertical post. This part of the antenna is responsible for the radiation. The current on the top hat decreases rapidly from the center to the edge. By increasing the size of the top-hat the antenna resonant frequency moves towards lower frequencies. Thus, increasing the top-hat radius effectively reduces the antenna height. At the same time the real part of the impedance decreases when the antenna height is reduced. Therefore, a compromise is needed between antenna height and good matching.

The equivalent circuit model of a top-hat monopole is as shown in Fig. 2 where C_s is the capacitance between the ground plane and the top-hat, R_d the radiation resistance of the driven post, L_d the inductance of the driven post with the hat, and C_d the capacitance between the driven post and the
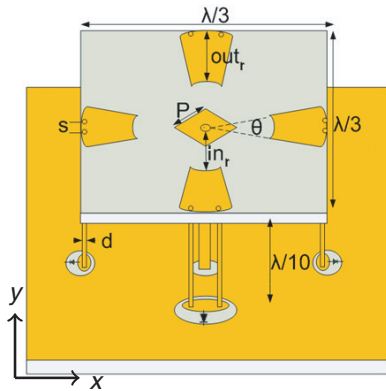
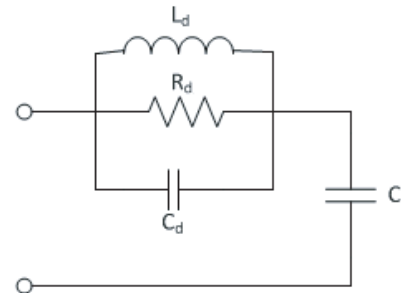**Figure 1.** Perspective view of the single reconfigurable antenna.

Figure 2. Equivalent circuit model of top-hat monopole antenna.

ground. Since the input impedance of the monopole is now very low it would be advantageous to use additional shorting post establishing a folded monopole and thus increasing the impedance. However, in case of this design it is not needed since the parasitic elements increase the input impedance.

The choice of the top-hat shape for driven element is based on the study considering which geometric shape offers a smaller size for the same resonant frequency, and at the same time offers better antenna performance in terms of bandwidth and gain. Analysis considers three possible shapes for the driven element top-hat. The dimensions of the three shapes square, circle and ellipse were optimized for the center frequency of 2.6 GHz. The square shape top-hat with dimensions 13 mm × 13 mm performs the best of all three evaluated shapes. The reflection coefficient plotted in Fig. 3 shows that improved matching and bandwidth can be obtained using square shape. It offers twice as much bandwidth as elliptical (11 mm and 8.5 mm, major and minor axis respectively) top-hat and 20% more than a circular (8.6 mm radius) top-hat.
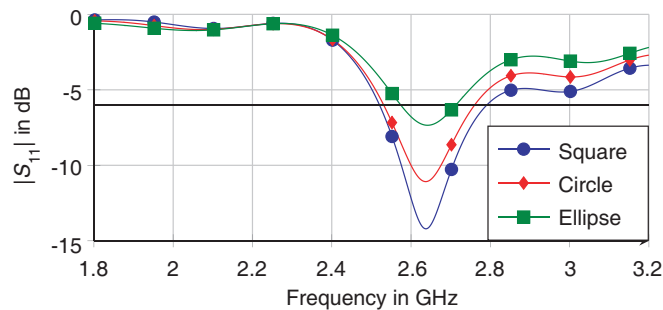

Figure 3. Reflection coefficients of the top-hat monopole for different top-hat shapes.

2.2. Parasitic Element Design

In order to obtain reconfigurable directive patterns parasitic elements are placed in vicinity of the driven element (see Fig. 1). The parasitic elements resemble the primary radiator in their form. They comprise as well of vertical posts with a top-hat. The equivalent circuit model of the parasitic element is the same as the one of the top-hat monopole and thus the parameters can be determined in the same way. However, the resonant frequency of the parasitic element is designed to be slightly lower than that of the driven element. This allows the parasitic element to act as a reflector.

The form of top-hat used for parasitic elements differs from the one used for primary radiator. A sector-ring shape is chosen for the parasitic elements (see Fig. 1) as it offers a more compact antenna size than the rectangular shape. Tuning the element to required resonant frequency involves changing

the angle θ and the radius out_r. Therefore, the radius can be kept small, while increasing the angle θ. Thus, antenna dimensions can be reduced. The parameters are set to $\theta = 17°$ and $out_r = 10\,\text{mm}$ to achieve reflector behavior of the parasitic elements. Another important design issue are the vertical posts. In case of parasitic elements there are two post per element. Introducing second post adds inductance and capacitance, thus reducing the size of the element further. Moreover, unlike in case of primary radiator, the posts are placed on the outer side and not in the middle of the element. Thus, not only the resonant frequency is reduced but also the antenna efficiency increases.

The distance between the parasitic element and the driven element can also contribute to size reduction. Reducing the distance in_r increases the coupling between the driven and parasitic element causing lowering of the resonant frequency. Thus, the hat dimensions or the vertical height can easily be reduced to obtain the desired frequency. However, this causes a reduction in antenna performance in terms of efficiency and gain. As a trade-off between antenna size and and performance in_r is set to $12\,\text{mm}$. Thus, the distance between the phase center of the primary radiator and the one of a parasitic element is about $0.14\lambda_0$.

2.3. Pattern Reconfiguration

A reconfigurable antenna for automotive application should be able to direct its main beam in the driving direction and against the driving direction as discussed in the introduction. Furthermore, beams in direction perpendicular to the driving direction are as well necessary for system performance. That can be achieved by using four parasitic elements placed around the primary radiator as shown in Fig. 1. A bigger number of parasitic elements does not increase the antenna flexibility, while decreasing the antenna efficiency. A parasitic element acts like a reflector when shorted to the ground and acts like a director when not shorted to the ground.

In order to alter between different patterns, a change in the behavior of respective parasitic elements from reflector to director is needed. Therefore the elements have to be connected to the ground with electrical switches, in this case p-i-n diodes are chosen due to the low price and low switching time. Considering the structure of the antenna, integration of the p-i-n diodes for switching of the parasitic element with two shorting wires becomes difficult. The possible solution is etching an elliptical slot in the ground plane and connecting the two shorting wires to a metallic pad placed in the middle of the slot as shown in Fig. 4(a). For each parasitic element there is one p-i-n diode placed between the pad and the ground. When the p-i-n diode is switched ON, the current on the corresponding shorting wires is around $-80°$ out of phase with the current flowing in the feeding monopole. Considering the distance between primary radiator and parasitic elements of $0.14\lambda_0$, constructive interference in direction of primary radiator is observed (parasitic element acts as a reflector). If the p-i-n diode is switched OFF, the parasitic element is around $140°$ out of phase with fed monopole. Thus, a constructive interference

(a)   (b)
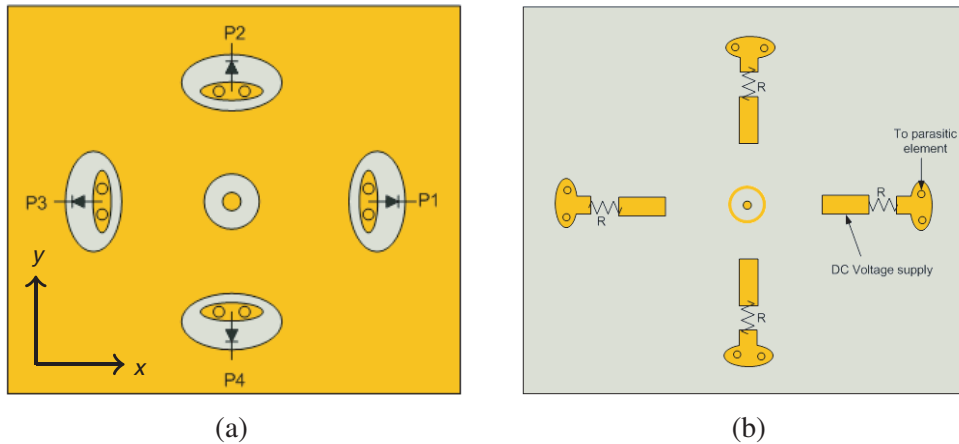
Figure 4. Layout of the ground plane with shorting pads, p-i-n diodes and DC feeding lines. (a) Top view. (b) Bottom view.

in direction of the parasitic element can be observed.

The elliptical pads (see Fig. 4(a)) are connected to metallic pads placed underneath the ground plane (see Fig. 4(b)) using vias. Hence the DC signal can be supplied to the p-i-n diodes. Apart from metallic pads there are also metallic strips and resistors comprised in the DC feeding network (see Fig. 4(b)). The task of the resistor is to block the high frequency signal from entering the DC supply. The resistance value of $5\,\mathrm{k}\Omega$ is chosen, thus the DC control signal is set to $5\,\mathrm{V}$ to switch the diode ON and $0\,\mathrm{V}$ for the diode in OFF state.

The final antenna is a 3D structure with the top-hats of the primary radiator and of the parasitic elements separated from the ground plane by a height $h = 11.5\,\mathrm{mm}$ (see Fig. 1). The top-hat and parasitic elements are printed on Rogers RT5880 substrate with permittivity $\varepsilon_r = 2.2$ and a thickness of $0.508\,\mathrm{mm}$. A small ground plane is printed on FR-4 substrate material with permittivity $\varepsilon_r = 4.3$ and a thickness of $1.6\,\mathrm{mm}$. The antenna is fed by a standard $50\,\Omega$ coaxial cable which is thread through the hole in the ground plane. A large ground plane of about $500\,\mathrm{mm} \times 500\,\mathrm{mm}$ is used for the antenna simulation to emulate the possible large ground plane of the car roof.

There are 10 different patterns that can be generated if four parasitic elements are placed in the vicinity of the primary radiator. Compared to [14] where six parasitic elements are used to generated six patterns, the antenna presented in this work offers more flexibility while being more compact. The possible switch configurations are presented in the Table 1. As discussed in the introduction the antenna patterns should cover the driving direction (positive x), the opposite direction (negative x) and directions to the left and right of the car ($\pm y$ direction). These patterns are realized by states 1–4 and the horizontal cuts for this states are presented in Fig. 5(a). In some cases it might be important to cover the $\pm$ driving direction or left/right direction simultaneously, this cases are realized by states 5 and 6 (see Fig. 5(b)). Additionally, the antenna can generate patterns directed towards the corners of the car roof $\psi = 45°, 135°, 225°$ and $315°$. These patterns are realized by states 7–10 (see Fig. 5(c)).

Table 1. Switch combinations for different reconfigurable states.

State	Diode	P1	P2	P3	P4
1	ON	ON	OFF	ON	
2	OFF	ON	ON	ON	
3	ON	OFF	ON	ON	
4	ON	ON	ON	OFF	
5	ON	OFF	ON	OFF	
6	OFF	ON	OFF	ON	
7	ON	ON	OFF	OFF	
8	OFF	ON	ON	OFF	
9	OFF	OFF	ON	ON	
10	ON	OFF	OFF	ON	

The performance of the antenna can be better observed in Fig. 6. The beam for states 1–4 has its maximal gain of $6.9\,\mathrm{dBi}$ at $\theta = 60°$. The half power beamwidth (HPBW) covers the angular range of $\pm 61°$ in azimuth and $\theta = 46°$ to $80°$ in elevation (see Fig. 6(a)). The front-to-back ratio is $3.5\,\mathrm{dB}$. However, similar patterns could be obtained by activating only one diode instead of three, the gain and matching would deteriorate. The gain of the antenna with three of the diodes switched ON is $6.9\,\mathrm{dBi}$ while for only one diode switched ON it is $4.3\,\mathrm{dBi}$, thus a reduction in gain of $2.6\,\mathrm{dB}$ is observed. There are two beams pointed in opposite directions in states 5 and 6 and maximal gain of $5.7\,\mathrm{dBi}$ at $\theta = 60°$ is achieved. The HPBW covers the angle range of $\pm 53°$ in azimuth and $\theta = 49°$ to $79°$ in elevation (see Fig. 6(b)). The difference between the gain in desired direction and the orthogonal direction is $4\,\mathrm{dB}$. And finally for the states 7–10 beam with maximal gain of $7.2\,\mathrm{dBi}$ at $\theta = 60°$ is obtained. This gain value is higher than the one for states 1–4. It can be easily explained by the radiation towards the

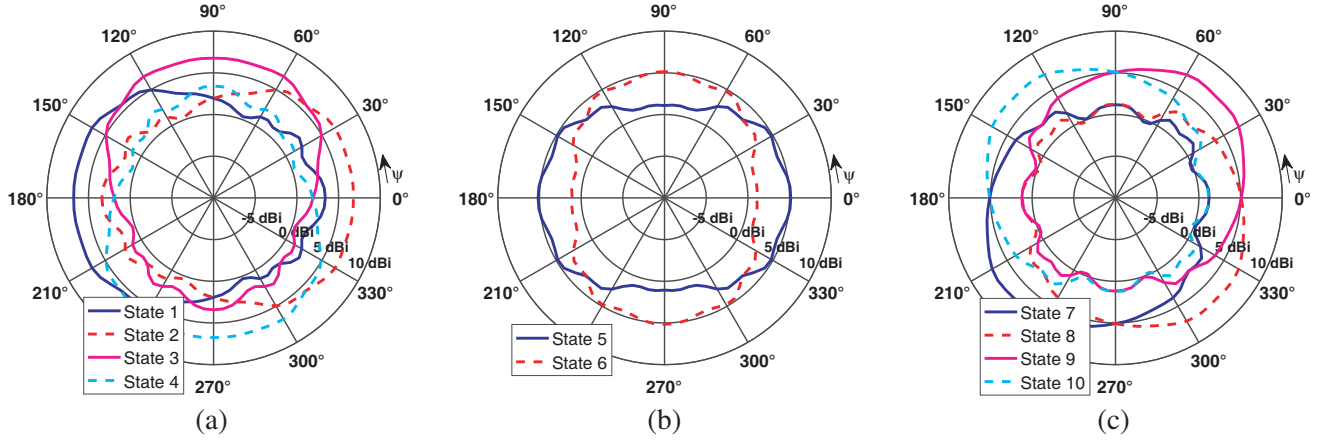**Figure 5.** Horizontal cuts of the radiation patterns at 2.6 GHz for elevation angle $\theta = 60°$. The right sides of the plots ($\psi = 0°$) coincide with driving direction.
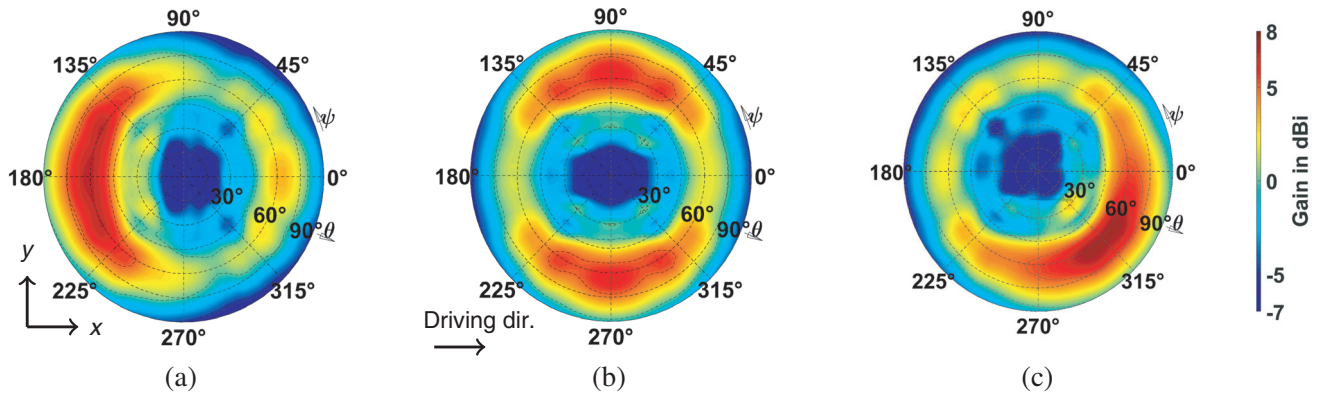

Figure 6. Simulated 3D antenna radiation patterns at 2.6 GHz.

corner of the car roof and thus larger ground plane dimension at the diagonal. The HPBW covers the angle range of $\pm 59°$ in azimuth and $\theta = 48°$ to $78°$ in elevation (see Fig. 6(c)). The front-to-back ratio is 6.1 dB. Simulated total antenna efficiency has values between 70% for states 7–10 and 77% for states 5 and 6.

Figure 7 presents simulated reflection coefficients of the reconfigurable antenna. It can be seen that the best matching is obtained for states 1–4, in which case three diodes are switched ON. The curve is also shifted towards higher frequencies compared to the curves for states 5 and 6, and 7–10. In general it is observed that for states in which two diodes are ON worse matching occurs.

3. RECONFIGURABLE MIMO ANTENNA

Wireless communication systems that support very high transmission rate are anticipated in 5G. The 5G proponents are convinced that the high-performance cellular network will be able to offer similar functionality as dedicated car-to-car communication [19]. In order to provide enough throughput yet a wider use of MIMO systems is anticipated. The use of pattern reconfigurable MIMO antenna systems allows further improvements in channel capacity and increased data transmission rate.

3.1. Antenna Configuration

In order to create a MIMO antenna two reconfigurable antennas as presented in Section 2 are placed next to one another along driving direction (see Fig. 8). The two antennas share a common ground plane
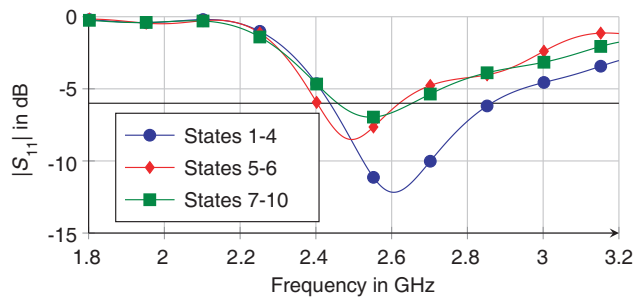
Figure 7. Input reflection coefficients for different reconfigurable states of the antenna.
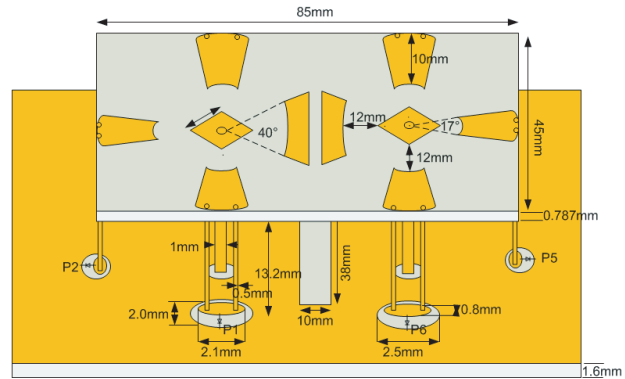

Figure 8. Configuration of the MIMO reconfigurable antenna (perspective view).

and the phase centers of both antennas are separated by about $\lambda_0/3$. The small separation was chosen in order to obtain a compact design suitable for automotive application. The reconfiguration of adjacent parasitic elements positioned between the driven elements of both antennas becomes useless, since the antennas shadow one another. Therefore, both parasitic elements are designed to act as reflectors. In order to reduce the coupling between these elements the vertical posts are removed. Therefore, the size of these two parasitic elements is increased so that they are still able to act as a reflector. Furthermore, by decreasing their radius it becomes possible to place the antennas closer together. An increase in size of this elements is achieved by increasing the angle of the arc section of the element which is now $\theta = 40°$, more than double the original value (see Fig. 8).

However, the closer the antennas are placed to each other, the more coupling between both antennas is observed. Furthermore, due to the coupling between the antennas, the radiation efficiency of both antenna is reduced. In the worst case the coupling between the two antennas' input ports is $-9\,\text{dB}$. This value is unacceptable since not only antenna's performance is deteriorated but also the front-ends of the antennas could be damaged by a strong signal coupled from one port to the other. Therefore, a decoupling structure should be used to solve this problem. The mutual coupling between the antennas is caused by free-space radiation and the current on the common ground plane. In order to reduce the first cause a parasitic resonator can be used [20]. This solution is however hard to apply in this case. Various techniques reduce mutual coupling by modifying the ground current since it has dominant contribution to mutual coupling [21–23]. In this case slots are cut in the ground plane. These techniques are simple and cost effective to implement since it only involves etching a structure on the common ground plane of the antennas.

3.2. Decoupling Structures

In order to ensure low mutual coupling between the antennas, three different decoupling structures placed on the ground plane (see Fig. 9) were tested and compared.

The first possibility is use of an H-shaped structure as presented in [21]. It consists of three slits of length k and width w interleaved with metallic strips of width s and length k which are etched in the middle of the ground plane (see Fig. 9(a)). The strips can be thought of as capacitors, some additional inductance is introduced by the central small connecting strip of width c. Therefore, the structure is equivalent to a band-stop filter based on a parallel LC network. The structure reduces the surface current flowing through it by trapping most of the surface current on the side of the radiating antenna and thus reducing mutual coupling. The structure is optimized to have a band-stop region from $2.2\,\text{GHz}$ to $2.75\,\text{GHz}$ with a mutual coupling across the band lower than $-10\,\text{dB}$ when the design parameter values are $k = 19\,\text{mm}$, $s = 0.5\,\text{mm}$, $w = 0.5\,\text{mm}$, $c = 1.5\,\text{mm}$.

The structure of the dumbbell, as presented in [22], etched on the ground plane is as shown in Fig. 9(b). It consists of a dumbbell rectangular head of length a and width b, slot length between the dumbbell d and a slot width s. The dumbbell structure is designed so that the resonant frequency of
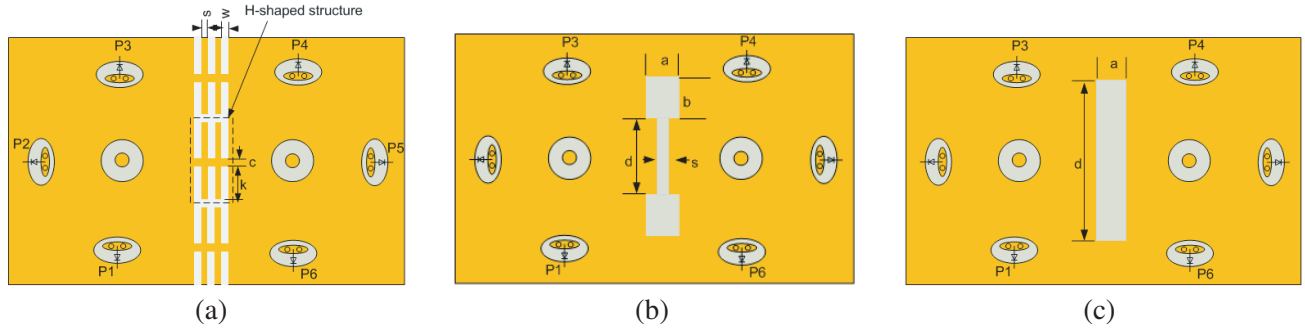
Figure 9. Evaluated decoupling structures. (a) H-shaped. (b) Dumbbell. (c) Slotted ground plane.

the MIMO antenna falls in its band gap. Thus the dumbbell structure reduces mutual coupling by suppressing the surface wave. The design parameter values are $a = 5\,\text{mm}$, $b = 5\,\text{mm}$, $d = 18\,\text{mm}$, $s = 1\,\text{mm}$.

The third option is to use a slotted ground plane (SGP) as discussed in [23]. The slot (see Fig. 9(c)) is designed to resonate at nearly the design frequency of the antenna and due to its increased width a relatively broad band is covered. The energy instead of being transmitted from one to the other antenna is stored in the slot and thus the mutual coupling between the antennas is reduced. Slots width a is $10\,\text{mm}$ and length d is $38\,\text{mm}$.

The effects of the decoupling structures on the performance of the antenna are finally compared. However, the decoupling structures reduce the performance of the antenna in terms of gain and radiation efficiency, and at the same time it improves the isolation between the ports. The structure with higher decoupling leads to a lower antenna gain. Therefore, the resonance of the decoupling structures is placed below the center frequency of the MIMO system, and a trade-off is reached between degree of mutual coupling reduction and antenna performance. All the structures fulfill their task, yet the SGP offers the best isolation of around $25\,\text{dB}$ (see Fig. 10) and lowest influence on antenna radiation.
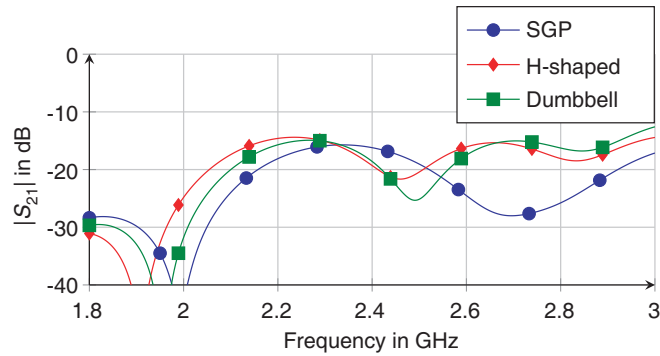

Figure 10. Isolation between MIMO antenna ports for different decoupling structures.

3.3. Reconfigurable Patterns

The p-i-n diode configuration of the MIMO antenna is as shown in Fig. 9. The mechanism of the p-i-n diode switching is the same as that used for a single antenna, thus switching each p-i-n diode ON connects the parasitic element to the metallic ground plane. Since, as discussed at the beginning of this section, one diode per antenna is removed resulting in six diodes MIMO design. The two antennas are $180°$ symmetric in azimuth and thus most of the possible reconfigurable states are symmetric. The possible reconfigurable states of interest are as listed in the Table 2. Diodes P1, P2, P3 are used for pattern reconfiguration of the first antenna (A1) whereas diodes P4, P5, P6 are used for second antenna (A2).

Table 2. Switch combinations for different states of MIMO antennas.

Diode State	P1	P2	P3	P4	P5	P6
1	ON	OFF	ON	ON	OFF	ON
2	ON	OFF	ON	ON	ON	OFF
3	ON	OFF	ON	OFF	ON	ON
4	OFF	ON	ON	ON	OFF	ON
5	ON	ON	OFF	ON	OFF	ON
6	ON	ON	OFF	OFF	ON	ON
7	OFF	ON	ON	ON	ON	OFF
8	ON	ON	OFF	ON	ON	OFF
9	OFF	ON	ON	OFF	ON	ON
10	ON	OFF	ON	OFF	ON	OFF
11	ON	OFF	ON	OFF	OFF	ON
12	OFF	ON	OFF	ON	OFF	ON
13	ON	OFF	OFF	ON	OFF	ON
14	ON	OFF	ON	ON	OFF	OFF
15	OFF	OFF	ON	ON	OFF	ON

Similar to the single antenna, the MIMO antenna patterns cover relevant directions like ± driving direction or left/right direction. Since the center parasitic elements acts as reflectors, there is no radiation pattern directed towards the opposite driven element. The radiation patterns of state 2, state 3, state 4 and state 5 are rotationally symmetric in azimuth. Also the radiation patterns of state 6 and state 7 are 180° rotationally symmetric in the horizontal plane, likewise patterns of state 8 and state 9. Furthermore, the patterns covering left/right direction (states 10 and 12) and directions towards corners of the car roof (states 11, 13, 14 and 15) can also be generated. Compared to the single antenna from Section 2, each of MIMO antennas cannot generate a radiation pattern simultaneously covering of ± driving direction. However, the MIMO system can still generate this pattern. Considering the symmetric nature of the antenna, six representative antenna states are selected and presented in Fig. 11. For each state the patterns of antennas A1 and A2 are displayed.
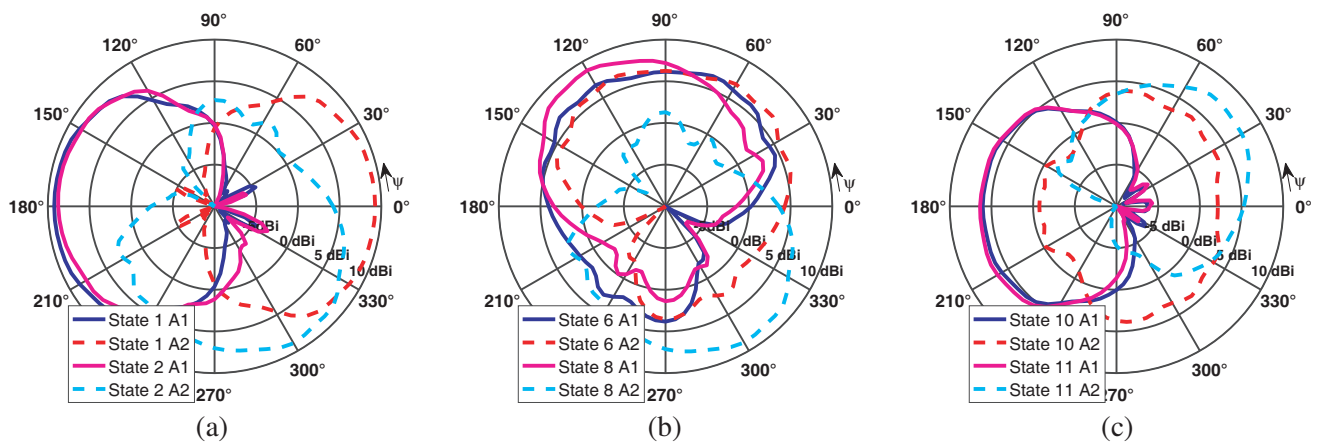

Figure 11. Simulated horizontal cuts of the radiation patterns at 2.6 GHz for elevation angle $\theta = 60°$. The right sides of the plots ($\psi = 0°$) coincide with driving direction. (a) States 1 and 2. (b) States 6 and 8. (c) States 10 and 11.

Due to the small distance between the antennas, the active parasitic element of the adjacent antenna affects the radiation pattern of the considered antenna. The least influence can be observed for state 1 (see Fig. 11(a)), in which case P1 and P5, placed opposite to each other, are OFF. A shift in the main beam radiation direction in azimuth from 270° to around 300° can be observed for antenna A2 in state 2 (see Fig. 5(a)). It is due to the active parasitic element P6 of the second antenna. Similar shift is also observed for states 3 to 9. Therefore, the main problem of the MIMO antenna design is the modification of the main beam direction due the presence of adjacent parasitic elements of the second antenna. The highest gain is obtained by antennas A1 and A2 in state 1 (± driving direction) and it is about 9.2 dBi. High gain is also observed in left/right direction for states 2 to 9 and its value is about 8.6 dBi. Slightly lower gain 7.6 dBi is generated in directions of the corners of the car roof in states 11, 13, 14 and 15. In states 6 and 7 a maximal gain of 6.6 dBi is observed in left and right direction. In states 10 and 12 a gain of 4.6 dBi is observed in left/right direction, while around 6.5 dBi it is observed in ± driving direction.

The S-parameters of the MIMO antenna are shown in Fig. 12. The matching of the antenna for all states is improved using the decoupling structure. The return loss of about -17 dB is achieved with the decoupling structure as compared to the return loss of about -10 dB without decoupling structure. The bandwidth at -6 dB for the return loss is from about 2.4 GHz to 2.8 GHz for all states. The matching for states 10 and 11 and the analogous states is worse than that for the other states. This is because diodes P4 and P6 are OFF and the two parasitic elements of antenna 2 that are closest to antenna 1 are not shorted. In this case they have most influence on the S-parameters at both antenna ports. This behavior could be improved by increasing the overall antenna size; however, the slightly worse matching is accepted as antenna miniaturization was important design goal. All the states show a good isolation of at least -14 dB at the design frequency.
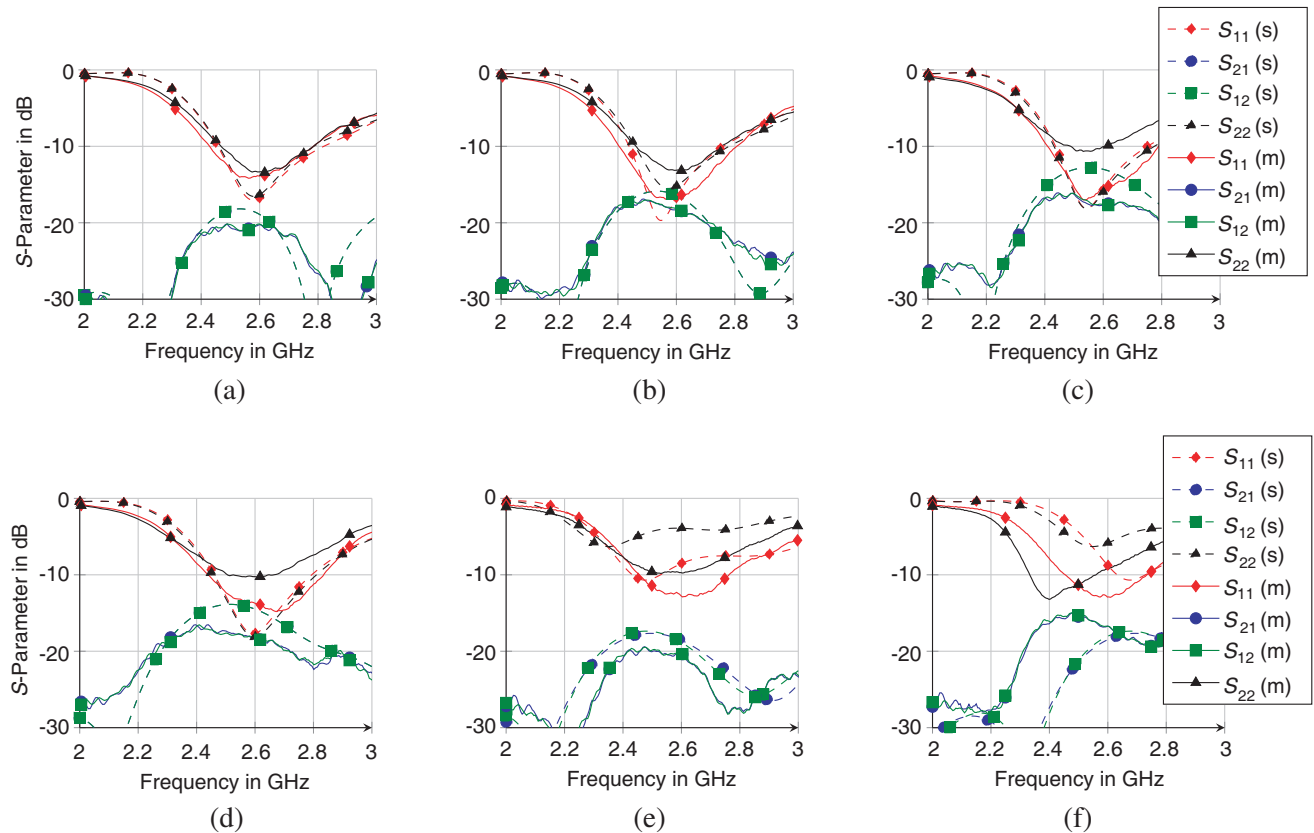

Figure 12. Simulated and measured S-parameter for the MIMO antenna. (a) S-Parameters for state 1. (b) S-Parameters for state 2. (c) S-Parameters for state 6. (d) S-Parameters for state 8. (e) S-Parameters for state 10. (f) S-Parameters for state 11.

4. ANTENNA MEASUREMENT AND EVALUATION

4.1. *S*-Parameter and Pattern Measurement Results

In the next step a prototype of the antenna (see Fig. 13) is fabricated and measured. The p-i-n diode used is BAP64-02 from NXP. The measured input reflection coefficients of antennas 1 and 2 in different states correspond well with the simulation (see Fig. 12). A slightly worse measured reflection coefficient and thus bigger discrepancy between measurement and simulation is observed for antenna 1. It can be explained by imperfections in manual fabrication. However, if -6 dB bandwidth is considered, the antenna still covers the frequency range from 2.4 GHz to 2.8 GHz. The measurement results show a very good isolation in all states. Its value is better than the simulated one (see Fig. 12) which can be partially explained by worse reflection coefficients of antenna 1.
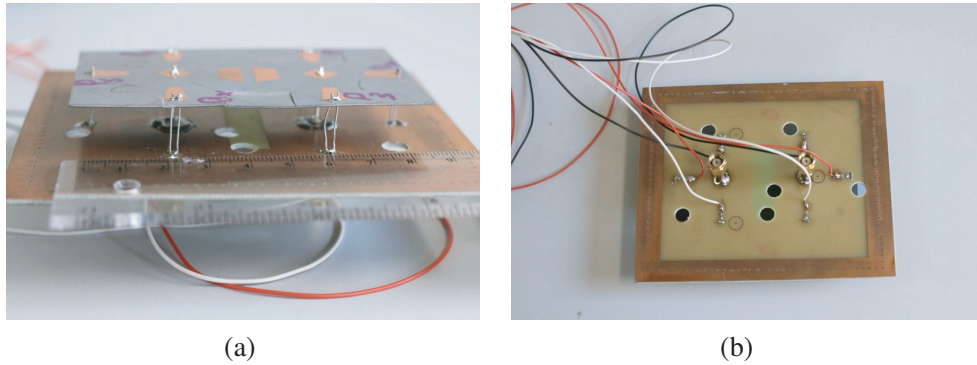

(a)   (b)

Figure 13. Prototype of MIMO antenna. (a) Top view. (b) Back view.

In the next step calibrated gain pattern measurements are performed inside an anechoic chamber. For measurement purposes the prototype is attached to a large ground plane with a size of 500 mm $\times$ 500 mm. The drill holes visible in Fig. 13 are necessary in order to mount the antenna on the rotary tower inside the anechoic chamber. The states of the pattern reconfigurable antenna are switched by connecting the p-i-n diodes to a DC-power supply, as explained in Section 2.

The measured patterns are presented in Fig. 14. Comparing the simulated and measured gain values, the biggest difference can be observed for state 1 where instead of simulated 9.2 dBi gain 7.4 dBi is measured (see Figs. 14(a) and 14(b)). Nevertheless, it can be observed that the measurement results correspond very well to simulation results. Not only similar gain values are obtained for remaining states, but also the forms of the patterns correspond well.

4.2. Envelope Correlation Coefficient

The envelope correlation coefficient (ECC) is an important measure of antenna performance in MIMO systems. It is a metric used to measure the correlation between the antennas in the system and can be calculated from antennas S-parameters with formula given in [24].

$$\rho_e = \frac{|S_{11}^* S_{21} + S_{21}^* S_{22}|^2}{\left(1 - \left(|S_{11}|^2 + |S_{21}|^2\right)\right)\left(1 - \left(|S_{22}|^2 + |S_{12}|^2\right)\right)} \tag{1}$$

Table 3 shows the ECC value for representative antenna states. It can be seen that all values are below 0.015 what makes the antenna attractive for MIMO applications.

Table 3. Envelope correlation coefficient of different antenna states.

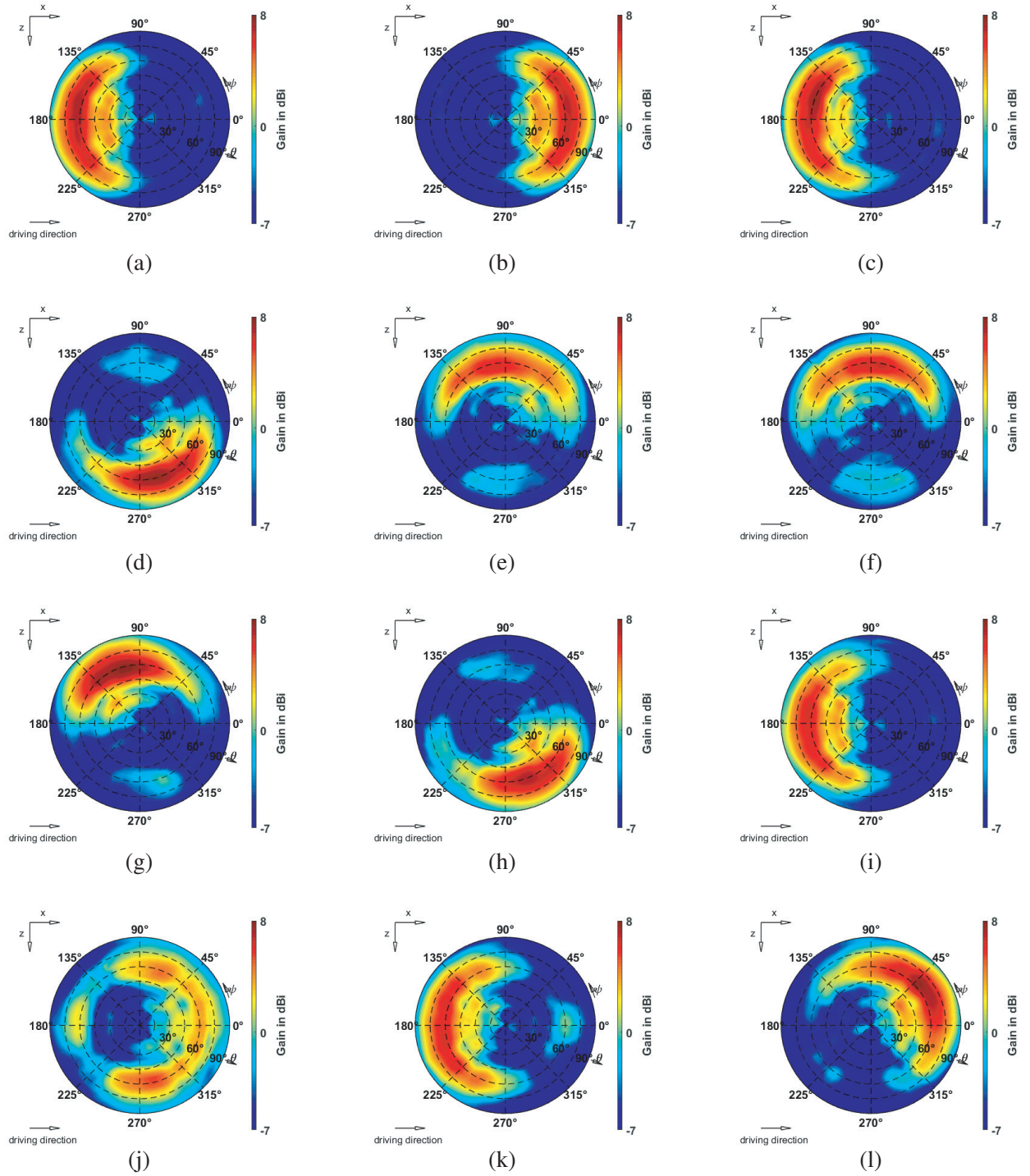| State	1	2	6	8	10	11
ρ_e	0.0143	0.0130	0.0097	0.0094	0.0086	0.0055

Figure 14. Measured 3D antenna radiation patterns at 2.6 GHz. (a) State 1, Antenna 1. (b) State 1, Antenna 2. (c) State 2, Antenna 1. (d) State 2, Antenna 2. (e) State 6, Antenna 1. (f) State 6, Antenna 2. (g) State 8, Antenna 1. (h) State 8, Antenna 2. (i) State 10, Antenna 1. (j) State 10, Antenna 2. (k) State 11, Antenna 1. (l) State 11, Antenna 2.

The ECC calculated from radiation patterns would be preferable since it is more exact and it is additionally possible to measure correlation between reconfigurable patterns. Furthermore a comparison between the the S-parameter and the radiation properties based ECC can be drawn. The radiation
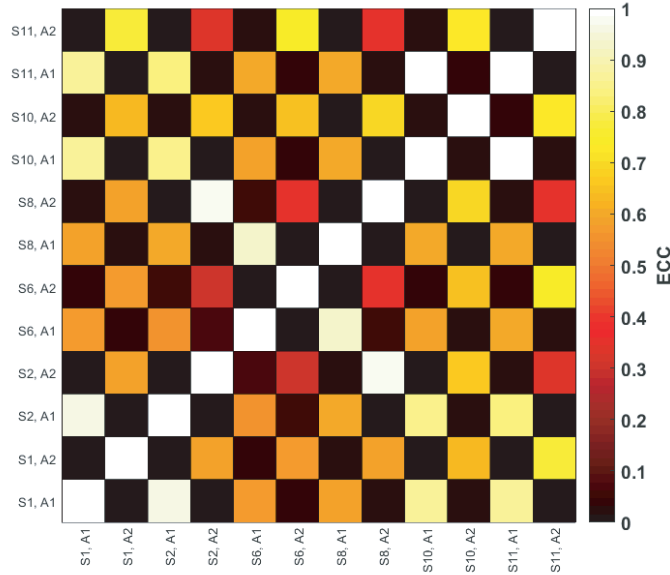
Figure 15. Envelope correlation coefficient calculated from radiation patterns for representative states of MIMO antenna at 2.6 GHz.

pattern based ECC can be calculated with formula given in [24].

$$\rho_e = \frac{\left| \iint\limits_{4\pi} \overrightarrow{F_1}(\theta, \psi) \cdot \overrightarrow{F_2}(\theta, \psi) d\Omega \right|^2}{\iint\limits_{4\pi} \left| \overrightarrow{F_1}(\theta, \psi) \right|^2 d\Omega \iint\limits_{4\pi} \left| \overrightarrow{F_2}(\theta, \psi) \right|^2 d\Omega} \tag{2}$$

The calculated values for pattern based ECC are presented in Fig. 15. For all states ECC value between antenna ports lower than 0.1 (black color in the plot) is observed, and thus the values are similar to the results obtained from S-parameter based calculation. The black chequered pattern distinguishable in Fig. 15 points out that the patterns created at both antenna ports are decorrelated very well. The decorrelation between different reconfigurable states at the same antenna port varies between low ECC for patterns pointing in different directions, e.g., antenna 2 in states 2 and 6 and high ECC for almost identical patterns, e.g., antenna 1 in states 1 and 2.

4.3. Comparison with Other MIMO Designs

A selection of previous work on reconfigurable MIMO antennas is given in Table 4. As seen, the proposed antenna offers higher gain and more reconfigurable states than the low-profile solution proposed

Table 4. Comparison of proposed MIMO antenna with other designs.

Publication	Max. meas. gain (dBi)	Freq. (GHz)	BW %	Size (mm^3)	States per port
Zhou [14]	3.5	2.28	-	$132 \times 66 \times 31$	6
Chamok [15]	10	5	14.7	$123 \times 10 \times 14$	3
Kishor [16]	below 0	2.28	7.2	$90 \times 30 \times 6$	2
Rhee [17]	5.4	5.2	4	$120 \times 70 \times 1.6$	3
This work	8	2.6	15	$85 \times 45 \times 13$	6

by Kishor and Hum [16] and Rhee et al. [17]. Furthermore, it is more compact and offers more gain, while having the same number of reconfigurable states as the design by Zhou et al. [14]. The reconfigurable parasitic array antenna proposed by Chamok et al. [15] has the same performance in terms of bandwidth and offers higher gain; however, the antenna proposed in this work outperforms it in terms of reconfiguration flexibility and compact construction.

5. CONCLUSION

This work presents a low-profile pattern reconfigurable MIMO antenna dedicated to automotive applications. The compact dimensions and reconfigurable patterns covering all directions crucial for automotive mobile communication make the antenna an attractive candidate to replace existing antennas. The mechanism of antenna's pattern reconfiguration is presented and discussed in detail. Different decoupling techniques are studied, and the best of them is proposed to improve the isolation between the antennas' ports. Finally, the measurement results of fabricated prototype are presented and the discussed. It is observed that the prototype generates the designed directivity patterns and offers high gain.

REFERENCES

1. Thiel, A., et al., "Automotive grade MIMO antenna setup and performance evaluation for LTE-communications," *2013 International Workshop on Antenna Technology (iWAT)*, 171–174, Karlsruhe, 2013.

2. Ekiz, L., A. Posselt, O. Klemp, and C. F. Mecklenbrauker, "System level assessment of vehicular MIMO antennas in 4G LTE live networks," *2014 IEEE 80th Vehicular Technology Conference (VTC2014-Fall)*, 1–5, Vancouver, BC, 2014.

3. Lankes, T., P. Turban, and F. Mierke, "Evaluation and optimization of LTE MIMO antenna configurations in automotive environment," *The 8th European Conference on Antennas and Propagation (EuCAP 2014)*, 1100–1104, The Hague, 2014.

4. Safin, E., R. Valkonen, and D. Manteuffel, "Reconfigurable LTE MIMO automotive antenna system based on the characteristic mode analysis," *2015 9th European Conference on Antennas and Propagation (EuCAP)*, 1–3, Lisbon, 2015.

5. Ross, P. E., "Europe's smart highway will shepherd cars from Rotterdam to Vienna," *IEEE Spectrum*, Dec. 30, 2014, [online], available: http://spectrum.ieee.org/transportation/advanced-cars/europes-smart-highway-will-shepherd-cars-from-rotterdam-to-vienna.

6. Ross, P. E., "World's first 5G-connected cars Demo'd in Korea," *IEEE Spectrum*, Nov. 16, 2016, [online], available: http://spectrum.ieee.org/cars-that-think/transportation/infrastructure/korea-demos-5gconnected-cars.

7. Reichardt, L., et al., "Using a synthesis methodology for the design of automotive antenna systems," *Proceedings of the European Conference on Antennas and Propagation, EuCAP 2013*, 1600–1604, Apr. 2013.

8. Mahler, T., L. Reichardt, C. Heine, M. Pauli, and T. Zwick, "Channel based design of systems with multiple antennas," *Progress In Electromagnetics Research B*, Vol. 64, 63–81, 2015.

9. Mahler, T., J. Kowalewski, B. Nub, C. Richt, J. Mayer, and T. Zwick, "Channel measurement based antenna synthesis for mobile automotive MIMO communication systems," *Progress In Electromagnetics Research B*, Vol. 72, 1–16, 2017.

10. Nguyen, V.-A., et al., "Four-port beam reconfigurable antenna array for pattern diversity system," *IET Microwaves, Antennas & Propagation*, Vol. 6, No. 10, 1179–1186, Jul. 2012.

11. Kang, H. and S. Lim, "Electric and magnetic loop mode pattern switchable antenna," *2012 International Symposium on Antennas and Propagation (ISAP)*, 1337–1340, Nagoys, 2012.

12. Zhang Y., et al., "A compact dual-mode metamaterial-based loop antenna for pattern diversity," *IEEE Antennas and Wireless Propagation Letters*, Vol. 14, 394–397, 2015.

13. Gyoda, K. and T. Ohira, "Design of electronically steerable passive array radiator (ESPAR) antennas," *IEEE Antennas and Propagation Society International Symposium, Transmitting Waves of Progress to the Next Millennium*, Vol. 2, 922–925, Salt Lake City, UT, USA, 2000.

14. Zhou, Z., R. S. Adve, and S. V. Hum, "Design and evaluation of pattern reconfigurable antennas for MIMO applications," *IEEE Transactions on Antennas and Propagation*, Vol. 62, No. 3, 1084–1092, Mar. 2014.

15. Chamok, N. H., M. H. Ylmaz, H. Arslan, and M. Ali, "High-gain pattern reconfigurable MIMO antenna array for wireless handheld terminals," *IEEE Transactions on Antennas and Propagation*, Vol. 64, No. 10, 4306–4315, Oct. 2016.

16. Kishor, K. K. and S. V. Hum, "A pattern reconfigurable chassis-mode MIMO antenna," *IEEE Transactions on Antennas and Propagation*, Vol. 62, No. 6, 3290–3298, Jun. 2014.

17. Rhee, C., et al., "Pattern-reconfigurable MIMO antenna for high isolation and low correlation," *IEEE Antennas and Wireless Propagation Letters*, Vol. 13, 1373–1376, 2014.

18. Artner, G., R. Langwieser, and C. F. Mecklenbruker, "Concealed CFRP vehicle chassis antenna cavity," *IEEE Antennas and Wireless Propagation Letters*, Vol. 16, 1415–1418, 2017.

19. Nordrum, A., "Autonomous driving experts weigh 5G cellular network against dedicated short range communications," *IEEE Spectrum*, May 3, 2016, [online], available: http://spectrum.ieee.org/cars-that-think/transportation/self-driving/autonomous-driving-experts-weigh-5g-cellular-network-against-shortrange-communications-to-connect-cars.

20. Minz, L. and R. Garg, "Reduction of mutual coupling between closely spaced PIFAs," *Electronics Letters*, Vol. 46, No. 6, 392–394, Mar. 2010.

21. Chiu, C.-Y., C.-H. Cheng, R. D. Murch, and C. R. Rowell, "Reduction of mutual coupling between closely-packed antenna elements," *IEEE Transactions on Antennas and Propagation*, Vol. 55, No. 6, 1732–1738, 2007.

22. Zhu, F.-G., J. D. Xu, and Q. Xu, "Reduction of mutual coupling between closely-packed antenna elements using defected ground structure," *Electronics Letters*, Vol. 45, No. 12, 601–602, Jun. 2009.

23. Caloz, C., H. Okabe, T. Iwai, and T. Itoh, "A simple and accurate model for microstrip structures with slotted ground plane," *IEEE Microwave and Wireless Components Letters*, Vol. 14, No. 4, 133–135, Apr. 2004.

24. Votis, C., G. Tatsis, and P. Kostarakis, "Envelope correlation parameter measurements in a MIMO antenna array configuration," *Int. J. Commun. Netw. Syst. Sci.*, Vol. 3, No. 4, 350–354, Apr. 2010.